HYDRODYNAMICS OF DISPERSED MEDIA
J.P. Hulin, A.M. Cazabat, E. Guyon, F. Carmona (eds.)

DYNAMICS OF WETTING : EXPERIMENTAL FINDINGS

M.A. COHEN STUART†, J.J. ELMENDORP* and S.M. TROIAN**

† Department of Physical and Colloid Chemistry, Wageningen Agricultural University, The Netherlands
* Koninklijke Shell Laboratoria, Amsterdam, The Netherlands
** Exxon Research and Engineering Co., Annandale, N.J., U.S.A.

ABSTRACT

Experimental studies of macroscopic liquid fronts spreading over solid surfaces are presented and discussed. On smooth, bare surfaces, experimental results agree well with a numerical solution of the hydrodynamic equations, which covers the whole range between capillarity-driven and gravity-driven processes. The behaviour of non-Newtonian liquids, like shear-thinning polymer solutions and elastic polymer liquids is also satisfactorily described. On rough surfaces, or surfaces covered by a preexisting liquid film, the spreading behaviour changes completely. In the case of a surfactant solution spreading on a preexisting water film, a fingering instability pattern develops rapidly; it is analysed in terms of surface tension gradients.

1. INTRODUCTION

The dynamics of wetting, i.e. the velocity at which a liquid front moves over a solid (thereby replacing a solid/vapour interface by a solid/liquid interface) is a subject of prime importance for numerous practical applications. On the other hand, it also appeals to the academic because it is very rich and full of surprises. We shall review here a number of recent experiments, inspired by preceding theoretical work such as that described in the previous chapter. The basic physics has been reviewed before by De Gennes *(1)*.

The main problem with wetting experiments is, that they are not so easily performed on the kind of idealised systems considered by the theory. Let us list a few complications.

(i) volatility. The very presence of a liquid/vapour interface implies that mass transport from the liquid to the dry solid surface may, in principle, take place through the vapour phase. Not only are such transports extremely difficult to control (see however the next chapter) also, they lead to temperature gradients, which in turn, may induce other gradients (e.g. surface tension gradients) thereby obscuring hydrodynamic aspects of the spreading process. Spreading in presaturated atmosphere may give reproducible results, but in that case spreading takes place over a preadsorbed liquid film.

A few experiments carried out by Lelah and Marmur *(2,3)* on spreading of water at various temperatures seem to provide evidence of deviations due to vaporization (or condensation). However, due to lack of control of the atmosphere around the spreading droplet, these results cannot be interpreted quantitatively.

(ii) contamination. The full understanding of wetting dynamics has to start from careful study of pure simple liquids. Unfortunately, trace contaminants are not always easily avoided, and they may have dramatic effects *(4)*. Contaminants may do either two things (i) they may adsorb onto the solid thereby changing its wettability (expressed through the spreading parameter S) or they may adsorb onto the liquid/vapour interface, causing changes in surface tension. The latter effect is interesting because it may lead to a Marangoni instability and enhanced spreading rate. In the abovementioned work of Lelah et al *(2)* there is a possible example of this in the spreading of alcohols, contaminated by atmospheric moisture. However, these authors discuss their data as if they are dealing with pure liquids. Below we discuss more careful recent work where a surfactant was added on purpose and spectacular but reproducible effects were observed.

The reader should be aware that, for liquids miscible with water, atmospheric moisture is a notorious contaminant. Another source of contamination is a reactive or impure solid, which leaches contaminant when in contact with the liquid. The effect of pH on the spreading rate of aqueous acid or alkali solutions on glass also reported in ref. *(2)*, would seem to fall into that category.

(iii) surface roughness. Most surfaces are more or less rough on microscopic (atomic) length scales. However, thermal fluctuations of the contact line are estimated to be much larger *(1)*, so that such roughness has probably no consequences for the wetting dynamics. Surface roughness in the micron-range, however, changes the wetting behaviour very dramatically; a rough surface presents itself to the liquid as a kind of 2-dimensional porous medium *(5)*.

We shall now discuss a number of experiments where complications were either avoided, or carefully controlled and accounted for. We begin with pure simple liquids; next, we consider non-newtonian (polymeric) liquids and finally we deal with surfactant solutions where a Marangoni effect seems operative.

2. SIMPLE PURE LIQUIDS

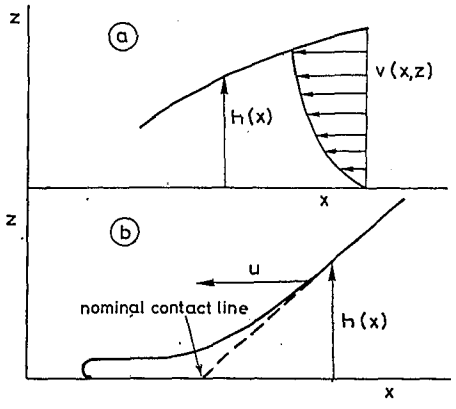

Fig. 1. (a) Velocity profile in a liquid film of varying thickness; definition of variables.
(b) Front of spreading liquid with precursor film (schematically).

Let us first recall the main theoretical predictions. At the macroscopic level, the advancing liquid front has the shape of a wedge bounded by the liquid/solid and liquid/vapour interfaces which intersect at the contact line under a well defined dynamic contact angle θ_d. Let us call-x the distance in the direction of motion, h(x) the height of the liquid above the solid surface at x, and z the vertical distance of a point in the liquid above the solid (fig. 1a). The average velocity, U(x,t) of the liquid will then satisfy *(1)*:

$$\eta\, U(x,t) = \frac{1}{3}\, h^2\, \frac{dp}{dx} \qquad (1)$$

where dp/dx is the pressure gradient in the direction of motion, and η the viscosity of the liquid.

Various forces contribute to dp/dx: capillary forces (Laplace pressure) which (for small θ_d) may be approximated by a term $-\gamma \frac{d^3h}{dx^3}$ where γ is the surface tension *(1)*; hydrostatic forces, given by $\rho g \frac{dh}{dx}$ where ρ and γ are liquid density and gravity acceleration, respectively *(6)*; and long range solid/liquid interaction forces denoted by a 'disjoining pressure' gradient $\frac{d\Pi(h)}{dx}$ *(1,7)*.

Now, from a macroscopic point of view, the latter forces vanish at the liquid surface. The remaining two terms, inserted into eq. 1, lead to an equation which various investigators have attempted to solve *(8,9)*. These attempts, however, met with the problem that the mathematical continuum model of the liquid wedge has a singularity at the contact line, because h vanishes there *(9)*. Approximations can be used to get around this and, fortunately, these do not seriously affect the result. Both analytical and numerical solutions were obtained *(8,10)*; as we will discuss below, the numerical approach also allows to incorporate non-newtonian effects, i.e. a shear rate dependent viscosity.The study of the equations led to two main conclusions :

(i) apart from logarithmic corrections the viscous force varies as θ_d^{-1} *(1)*

(ii) almost all the viscous dissipation comes from the region very close to the contact line, where h is small. The macroscopic shape of the liquid surface is therefore unaffected by the motion, i.e., it corresponds to the macroscopic, apparent contact angle as if it were static. There is, of course, a deformation zone around the contact line, but the width of that zone is of order $a\theta_d^{-2}$ *(1,11)* (a is a molecular size) which is for most cases negligibly small.

The above results are useful from a practical point of view. From the standpoint of fundamental physics, however, both the singularity alluded to above, and the neglect of disjoining pressure terms, are unsatisfactory. A major step forward was made by De Gennes and coworkers *(1)* who showed that the response of the liquid to a disjoining pressure is to form a thin precursor film which precedes the macroscopic front. In this picture, there is no singularity, since h is small but finite at the apparent (nominal) contact line (fig. 1b). A detailed discussion of thin wetting films follows in chapter 3.

2.1 Sessile drops

For small drops (or for drops surrounded by a fluid of equal density), the hydrostatic pressure plays a negligible role in the spreading rate. The solution of eq. (1) for that case is

$$Ca \equiv \frac{U}{\gamma}\,\eta \approx \theta_d^3 \qquad (2)$$

Here Ca is a dimensionless number called *capillary number*. Making use of the fact that the drop has a constant volume Ω, one can rewrite this in terms of the radius R(t) of the wetted spot:

$$R(t) \approx \Omega^{3/10}\left(\frac{\gamma\, t}{\eta}\right)^{1/10} \qquad (3)$$

Eq. 2 is the result first derived by Tanner *(8)* whereas Eq. (3) was straightforwardly deduced from *(3)* by De Gennes *(1)*. In view of our discussion in the introduction, we should measure spreading rates of oils (low volatility) under conditions of good (complete) wetting. With glass as the solid the liquid of choice is low MW polydimethylsiloxane (silicone oil) which has the property that it wets glass very well and is relatively insensitive to contamination. In addition, the viscosity η may be varied (by varying the MW), almost without changing γ. Hence, eq. (3) can be checked both for volume (Ω) and viscosity (η) dependence.

For the other case (large drops which spread mainly under their own weight) one finds :

$$R(t) \approx \Omega^{3/8}\left(\frac{\rho g t}{\eta}\right)^{1/8} \qquad (4)$$

a result first obtained by Lopez et al *(6)*. These results were checked in a study by Cazabat et al *(12,13)*.

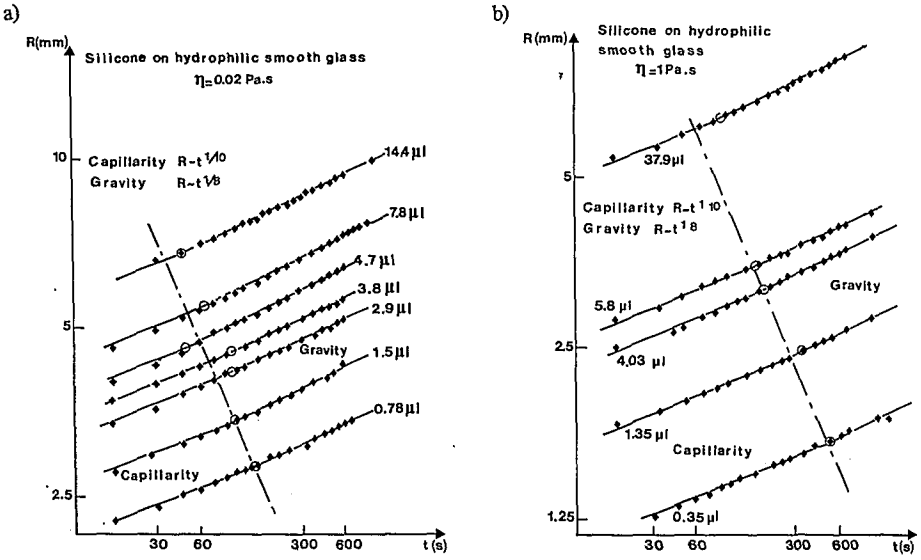

Fig. 2. Spreading kinetics of silicone oil on smooth hydrophilic glass surfaces (logarithmic plot). Solid lines are drawn according to theory. The approximate location of the transition is indicated by a circle. (a) η = 0.02 Pa.s. (b) η = 1 Pa.s. The dashed line separates the "capillary" and "gravity" regimes. From ref. *(56)*.

In Figs. 2 and 3, we reproduce the data plotted as log R vs log t, log R vs log Ω, respectively.

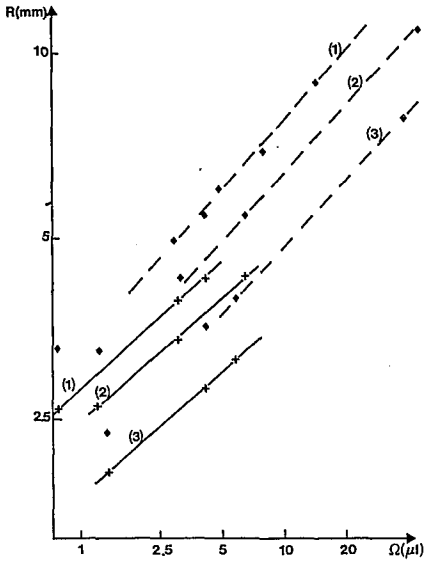

Fig. 3 The effect of the drop volume Ω on the rate of spreading on smooth surfaces: solid lines and crosses, drop size at 1 min (capillarity regime, slope $^3/_{10}$); dashed lines and diamonds, drop size at 7 min (gravity regime, slope $^3/_8$). (From *(56)*).

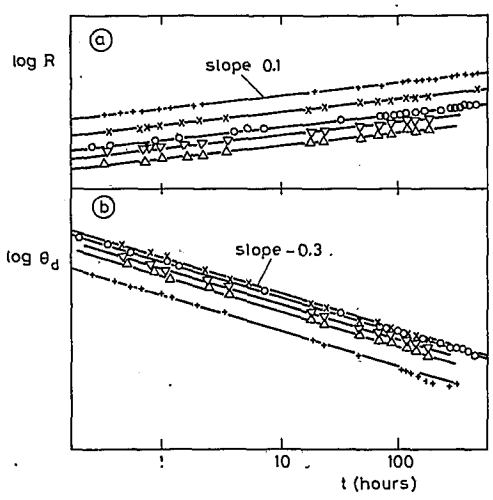

g. 4. Spreading of silicone oils (η = 426 Pa.s) on silicon wafers; (a) drop ... t; (b) apparent contact angle θ_d vs t. Different curves are for different drop volumes, ranging between 0.015 and 0.180 μl. (From ref. *(14)*).

As is immediately obvious, the data for small R agree with eq.3, (capillarity regime) whereas for larger, or more spread-out drops one finds agreement with eq. 4 (gravity regime). The dependence of R on Ω and on η were both found to be consistent with these two regimes. These results were further corroborated by Léger et al who studied both R and θ as a function of time for very small droplets of highly viscous silicone oils *(14)*. One such result is given in fig. 4. A problem is that in the experimental data of fig.2, the cross-over between the 'capillary' regime (small drops) and the 'gravity' regime (large drops) does not occur at a fixed value of R. A simple force balance argument would predict a crossover centered around an R value comparable to the capillary length, irrespective of drop weight *(15)*. Numerical calculations (see below) suggest that a fairly clear transition zone may indeed occur, but that its position is not at a fixed value of R *(16)*.

2.2 Pendant drops

For pendant drops which are sufficiently large, the hydrostatic term, which now opposes spreading, plays a major role. In order to obtain theoretical predictions one might take the naive approach and solve eq. 1, e.g., by numerical methods. However, this is very tedious. A simpler and more elegant way is to make use of the fact that the shape of the spreading droplet is the same as that of a static droplet with the same contact angle ('quasistatic approximation'). The shape of (static) pendant drops is a classical problem in capillarity with well-known solutions. Hence, in order to obtain the relation U(R), one first calculates θ from given values of R, Ω, ρ and γ, after which eq. (1) is used to obtain U. Such a scheme was used by Levinson et al *(17)* in a study of pendant silicone oil drops on glass, and good agreement was obtained between calculations and experimental data.

2.3 Sessile drops on rough surfaces

Spreading of silicone oils on glass surfaces with random roughness in the micron range was studied by Cazabat et al *(5,13)*. Qualitatively, the behaviour is very different from that on a smooth surface : part of the liquid spreads very rapidly in the roughness, thus forming a rim of wetted surface around the central cap. The results could be very well accounted for by considering the rough surface as a porous body, in contact with a reservoir (the central droplet). This model gives for the temporal evolution of the width of the rim, $\Delta R(t)$, a kind of Washburn equation:

$$\Delta R(t) \approx \sqrt{Dt} \qquad (5)$$

where D is a proportionality constant depending on viscosity (η) and roughness scale. When the reservoir is exhausted, the spreading slows down. Imposing the constraint of a constant amount of liquid in the roughness, one finds $R(t) \sim t^{1/4}$ which is consistent with the data obtained. It is interesting to note that the rate of spreading of the central drop initially continues to follow the 1/8 power law (eq. 2) : apart from the decrease of Ω due to the loss of liquid its behaviour is independent of the spreading process in the roughness. This situation is reminiscent of that of the drop and precursor film on a smooth surface, where the presence of the precursor film, although it solves a theoretical riddle, has no influence on the macroscopic spreading law.

3. NON-NEWTONIAN LIQUIDS

In this part we intend to explore to what extent non-newtonian liquid behavior affects the wetting dynamics. To this end, we incorporate shear-thinning behavior into the equations describing the flow, and perform numerical calculations to study the effects. We then consider experimental

data on shear thinning polymer solutions and a non-shear-thinning but elastic polymer liquid ('Boger fluid') for comparison with the numerical results.

3.1 Calculations

As pointed out above the Navier-Stokes equation leading to Eq. (1) can be solved numerically for the case where the pressure gradient is made up from a Laplace pressure and a hydrostatic term. The situation at the contact line is sketched in fig. 1b; it corresponds closely to the case studied by Tanner. We entirely neglect molecular interactions that are responsible for the precursor film but assume simply *a priori* that there is such a film and that it is flat and has a given, yet unknown thickness. The concave surface near the contact line generates a Laplace pressure:

$$\Delta p_L = \gamma\left(\frac{1}{R_1} + \frac{1}{R_2}\right) \tag{6}$$

where R_1 and R_2 are the radii of curvature of the liquid surface. Expressing R_1 and R_2 into the shape function h(x) of a droplet one obtains

$$R_1 = \frac{\left(1 + (dh/dx)^2\right)^{3/2}}{\frac{d^2h}{dx^2}} \tag{7a}$$

$$R_2 = \frac{R - x}{\frac{dh}{dx}}\left[1 + \left(\frac{dh}{dx}\right)^2\right]^{1/2} \tag{7b}$$

where R is the radius of the wetted area, and x = 0 is taken as the point where dh/dx becomes zero (Fig. 1b). As said above for small values of dh/dx and neglecting the curvature perpendicular to the plane of Fig. 1b, this can be approximated to : $\Delta p_L = \gamma \frac{d^2h}{dx^2}$. In addition to Δp_L, a hydrostatic pressure may of course be considered.

The flow maintained by the pressure gradient is given by the Navier-Stokes equation, which reads (in one dimension)

$$\frac{d(\Delta p)}{dx} = -\frac{d}{dz}\left(\eta \frac{dv}{dz}\right) \tag{8}$$

where v(x,z) is the local liquid velocity and z is the coordinate in vertical direction. Shear thinning effects appear in this equation as a shear-dependent viscosity. By way of example we used a modified Bird-Carreau viscosity model *(18)*

$$\eta = \eta_0\left[1 + \frac{1}{\dot{\gamma}_c}\frac{dv}{dz}\right]^n \tag{9}$$

where $\dot{\gamma}_c$ is a shear rate threshold value marking the onset of shear thinning.

The problem is further defined by the following boundary conditions. The thickness at x = 0 is arbitrarily set at some suitable value h_0 (see below). At x = R is the center of the macroscopic droplet, i.e. dh/dx = 0 again. Also, the function h(x) must satisfy the condition of volume conservation. The liquid velocity v is assumed to vanish at the solid surface z = 0 (no slip) while

the shear rate (and shear stress) must vanish at the liquid surface z = h.

The calculation is carried out as follows. Starting at x = 0, with dh/dx = 0 and an initial curvature value (d^2h/dx^2), the pressure gradient required for a given surface velocity v(h) is calculated by integrating the Navier-Stokes equation. Next, the curvature gradient that generates this pressure gradient is calculated from the derivative along x of the Laplace equation. From the first, second and third derivative of h(x) at x = 0, h at x = Δx is calculated. In this way, the shape h(x) of the droplet is calculated for a given initial curvature. Finally, an iterative scheme leads to the initial curvature that is consistent with the boundary conditions on the gross droplet shape (e.g., drop volume or contact angle, given by dh/dx at large x).

The film thickness at x = 0, h(0) is still indeterminate. However, it was checked that for h(0) varying over two orders of magnitude (5 – 500 nm), the dynamic contact angle varied at most 10% in absolute value. We are therefore confident in the reliability of our picture of the spreading dynamics.

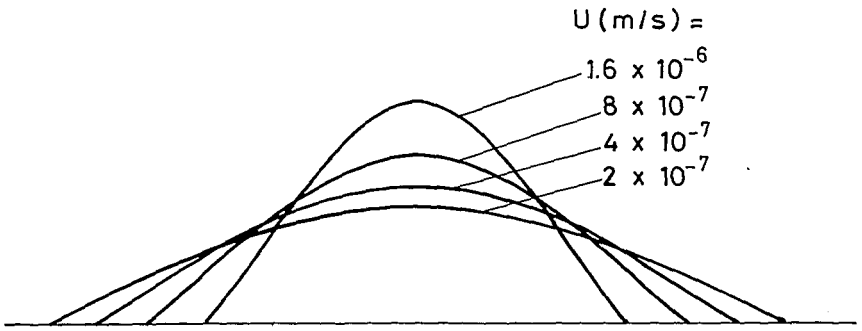

Fig. 5. Theoretical shape functions h(x) for a shear-thinning liquid droplet during spreading.

3.2 Numerical results

In fig. 5 we plot shapes of spreading droplet for various spreading velocities. For these pictures, a shear-thinning liquid satisfying the Bird-Carreau model was chosen with the following parameters (see eq. 9) : η_0 = 100 Pa.s, n = –0.64, $\dot{\gamma}_c = 0.135\ s^{-1}$. These values are those determined experimentally on a 3.4% solution of ultra-high MW polyisobutylene in isobutylene oligomer (see experimental section). The thickness of the pre-assumed precursor film, h(0), was arbitrarily set at 50 nm. The conspicuous feature of fig. 5 is the macroscopically concave shape of the edges of the droplet, especially at relatively high contact angles. In other words, the drop seems to develop a 'foot' which extends beyond the spherical cap shape usually observed for newtonian liquids. The calculations show that this foot is a consequence of the shear-thinning properties of the liquid; there is no need to invoke a 'slipping' process as proposed by De Gennes *(1)*.

In fig. 6 we plot the dynamic contact angle vs. capillary number as calculated for a newtonian fluid (silicone oil, η = 1 Pa.s) spreading under the combined action of gravity and surface tension. Appropriate values for the density and surface tension were used and h(0) was (arbitrarily) set at 50 nm. Therefore this result should be comparable to the experimental data shown in fig. 2b. It can be seen that, just as in the experimental data, the early stages of spreading are characterised by a slope of 0.33 which is just 'Tanner's law'. At low contact angle, however, the curve tends to a straight line with slope 0.41, which is what is expected for spreading under gravity.

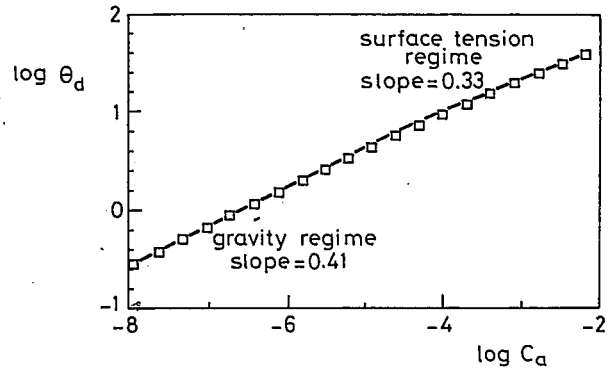

Fig. 6. Spreading rate (log θ_d vs log Ca) of a newtonian liquid (η = 1 Pa.s) calculated numerically. Both capillarity ("surface tension") and gravity regimes can be observed. Compare with the curves of Figs. 2 and 3.

Numerical results giving log θ_d as a function of log Ca appear in figs. 8-10, together with experimental data, and will be discussed in that context.

3.3 Experimental methods and materials

Spreading dynamics were studied in two ways. Spontaneous spreading of liquid droplets was chosen for its experimental simplicity, and forced wetting was studied by drawing tape vertically into a liquid at fixed, imposed velocity. Droplet spreading experiments were carried out on a flat substrate in a commercially available contact angle measuring instrument (Kruss), equipped with a video camera and recording system. For rapidly spreading drops, stroboscope illumination was used in order to prevent blurring of the video images. The tape immersion experiment, originally proposed by Burley and Kennedy *(19)*, was done by simply reeling up ordinary magnetic tape through a fairly large liquid reservoir. Observations were again recorded on video.

In order to investigate the influence of liquid elasticity on spreading kinetics, a Boger fluid, which is elastic but has constant viscosity, was prepared. Boger fluids exhibit normal stresses but no shear thinning since they consist of only a small fraction of high MW polymer in a highly viscous, (but newtonian) solvent *(20)*. The composition of our Boger fluid, made up of various polyisobutylene samples, is given in table 1.

	M_w	Boger fluid	Shear thinning solutions 1	2
*Oppanol B1	500 - 600	5.2 %	96.6%	
Oppanol B3		94.6%		
Oppanol B100	1-2 10^6			3.4%
Oppanol B200	3-5 10^6	0.2%	3.4%	
Decaline	-			94.6%

Table 1 composition of mixtures yielding shear thinning and Boger fluid solutions. (* BASF trademark)

Its rheological properties, i.e. its viscosity and normal stress, as a function of shear rate are summarized in Fig.7. Shear thinning solutions were also prepared from high MW polyisobutylene now dissolved at an higher concentration (3.4%) in decaline or PIB oligomer.

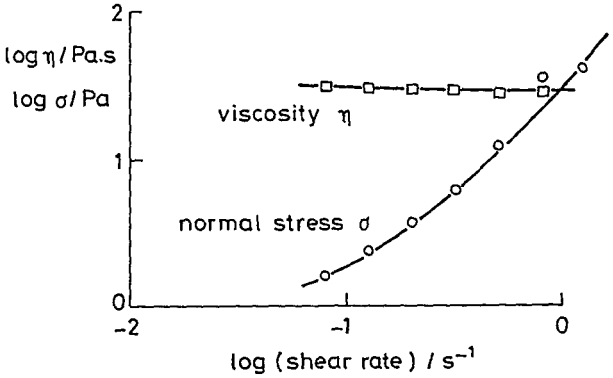

Fig. 7. Viscosity and normal stress of a Polyisobutylene-based Boger fluid.

Let us now discuss our experimental results : in fig. 8 we present dynamic contact angle data, plotted as log θ_d vs log Ca, for a newtonian silicone oil (open squares) and a shear thinning PIB solution.

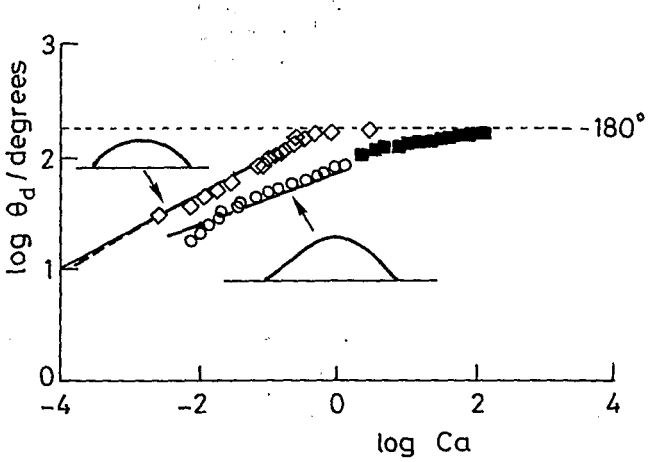

Fig. 8. Dynamic contact angle θ_d as a function of capillary number for a newtonian fluid (silicone oil, open squares) and a shear thinning PIB solution of high molecular weight measured by spontaneous spreading (open circles) and forced spreading (filled squares). Numerical results are represented by solid lines. The dashed line represents points for the Boger fluid (no experimental points shown).

Results from spontaneous spreading (open circles, low θ_d) and forced wetting (on the same liquid, solid squares) are shown. Numerical calculations, based on the rheological characteristics of the two liquids are represented by means of solid lines. The dashed line represents the Boger fluid.

Several observations can be made. First of all, θ_d for the shear thinning liquid increases much more gradually than that of the same newtonian liquid, even though both have the same zero-shear viscosity. The velocity at which θ_d approaches π is even shifted by at least two orders of magnitude. Secondly, the droplet shape of the shear-thinning liquid has a distinct foot, a feature which is absent in the shape of the newtonian droplet. Thirdly, the effect of normal stresses (Boger fluid) seems to be to slow down the spreading a little bit, but the effect is very small. Finally, we note here that the particular geometry of the spreading experiment has no influence on the spreading law: all points lie on a single curve.

Figure 9 gives some results obtained by forced wetting on both a newtonian (squares) and a shear thinning (circles) liquid. In this experiment, the substrate had cylindrical geometry (glass fiber). Calculated results are again shown by means of solid lines. Qualitatively, the same effect is observed as in fig. 8: shear thinning liquids spread faster (at given θ_d). We note in passing that the fiber diameter has a (small) effect on the results so that comparison between liquids of different type can only be made on fibers of the same diameter.

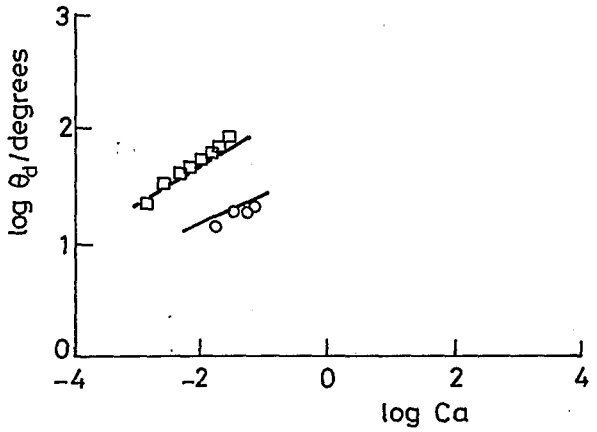

Fig. 9. Wetting of fibers by a newtonian (squares) and a shear thinning (circles) fluid. Theoretical results obtained numerically are represented by solid lines.

Finally in fig. 10 we give results for a system (Oppanol B_3 spreading on paraffin wax) where $\theta_d(Ca = 0)$ is not zero, but finite (partial wetting), namely 26°. At very low velocities, θ_d hardly differs from θ_d (Ca = 0), but as soon as $Ca > 10^{-3}$, θ_d increases strongly in the usual way. The theoretical result (solid curve) is in this case found by assuming that dh/dx at x = 0 does not vanish but has a finite value. This assumption may not be physically sound, but since there is still little dependence on the value of h(0), and since the agreement with experiment looks reasonable it seems to be an acceptable procedure.

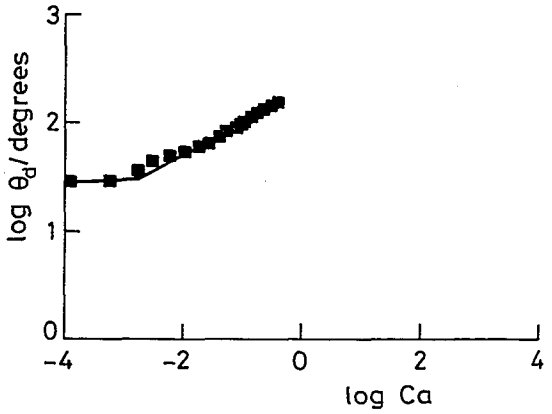

Fig. 10, Dynamic contact angle for liquid polyisobutylene (Oppanol B3) spreading on paraffin wax. The static contact angle equals 26°. Squares: experimental data. Solid curve: numerical theory.

4. FINGERING INSTABILITY OF SPREADING SURFACTANT SOLUTIONS : MARANGONI EFFECTS

In the previously mentioned studies of the dynamics of spreading of both Newtonian and non-Newtonian fluids, the macroscopic wetting process, whether forced or spontaneous, proceeds by the movement of a uniform and circular contact line. Unusual wetting behaviors can result during the spreading of a droplet of aqueous surfactant solution on a moist surface, leading to fingering of the apparent contact line. We recently reported experimental results *(21)* on a hydrodynamic instability, first observed by Marmur and Lelah *(22)*, which occurs when certain aqueous surfactant solutions (as well as other solutions discussed in *(21)*) spread on a surface premoistened with a thin film of water. The surfactant droplet has a lower surface tension than the thin layer of pure water on which it spreads. Upon deposition of the drop on the moist substrate, liquid in the thin water film is swept away from the vicinity of the drop causing thinning of the fluid layer near the drop edge, while a thickened rim, similar to a shock front, travels away from the drop. As this height profile develops, the remainder of the drop rapidly spreads into the thinned region and begins propagating fingers from the spreading front.

The surface coverage proceeds at a rate approximately an order of magnitude faster than in ordinary wetting, but it is non-uniform since the spreading drop leaves behind intricate dendritic-like patterns. The fingers appear to undergo lateral spreading, shielding, and tip-splitting *(23)*, processes known to occur in such instabilities as viscous fingering, diffusion limited aggregation and dendritic growth. The reason for this similarity initially eluded us since our system has no externally applied driving force, nor is it controlled by diffusive phenomena. In addition, the fluids used (aqueous surfactant solution with less than 0.1% surfactant by weight and pure water) are miscible and show negligible viscosity differences. Despite these differences, we have developed a theoretical model *(24)* which demonstrates that, in suitable asymptotic limits, the instability we observe can be explained in direct analogy to Hele-Shaw flow *(25)* and hence the connection to

those and other similar fingering patterns is made clear.

Details of the apparatus and further experimental results can be found in ref. *(21)*. Here we discuss just a few of our results. The experiments are performed in a sealed glass chamber at the bottom of which is placed a clean and dry glass slide. The thickness of the initial water film on the slide is controlled by monitoring the relative humidity in the chamber. A 2 μl drop of an aqueous solution of surfactant AOT (sodium bis-(2-ethylhexyl) sulfosuccinate), for example, in the concentration range 0.01 - 10 mM, is gently placed on the water moistened slide by means of a syringe introduced into a side port on the chamber, and the ensuing instability is recorded on videotape for later image analysis.

Shown in Fig.11 are two typical fingering patterns observed when varying the thickness of the initial film (Similar patterns can be gotten by varying the surfactant concentration also.) Our findings demonstrate that there is a critical water film thickness and a critical surfactant concentration needed in order to initiate the instability. Contrary to the results reported in ref. *(21)*, the surfactant solution spreads like a normal liquid and does not finger on a dry slide. In addition, the fingering process occurs both above and below the critical micelle concentration. The strong dependence of the rapid spreading and fingering on (a) the presence of the initial water film and (b) on the droplet surfactant concentration immediately suggests that the instability is driven by the Marangoni effect *(26)*. This effect describes how surface tension gradients (established in our experiments by variations in the surfactant concentration at the air-liquid interface) cause a shear stress in the fluid which induces flow in the direction of increasing surface tension. While the Marangoni effect has been studied in many situations leading to both stable and unstable flows, both our experiments and theoretical analysis indicate a new instability occuring at the spreading edge of a drop or thin film.

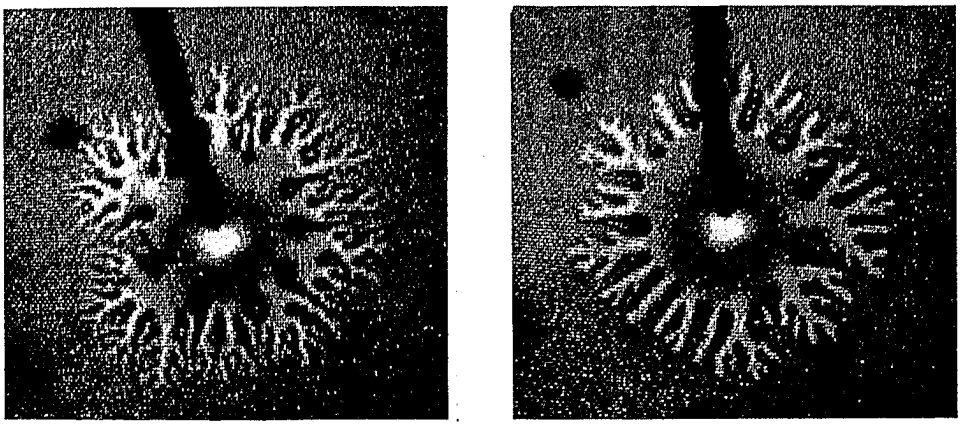

(a) (b)

Fig. 11 : Fingering of a drop of 1mM aqueous AOT spreading on an (a) thin (≈ 0.1 μm) and (b) thick (≈ 1 μm) water film. The outer radius of the drops is ≈ 0.9 cm. The dark needle corresponds to the syringe tip used for depositing the drops on the water film.

The onset of the instability is intimately connected to the presence of the long thinned region ahead of the drop which sustains the largest change in surface tension, from the value at the drop (40 dynes/cm for a 1 mM solution) to the value of the pure water film (73 dynes/cm). We can clearly visualize this region by coloring an AOT solution with naphthol blue-black dye, which behaves

similarly to a surfactant in this case. A dark rim of fluid spreads out radially a few millimeters ahead of the macroscopic contact line. Behind this rim a sharp depression in fluid height occurs and we see the fingers grow into this thinned region. Although difficult to photograph, the naked eye can clearly detect this same profile developing without the dye. The flow in this region is driven by the Marangoni effect which acts to spread the concentration jump established when the droplet is first placed on the water. Within the approximations discussed in ref. *(24)*, since the fluid velocity is directly proportional to the gradient in surface tension, and since protrusions in the apparent contact line experience a larger gradient than indentations, the finger tips move faster than the surrounding environment and in analogy to Hele-Shaw flow, the spreading front fingers .

To characterize the patterns, we have measured the growth rate of the fingers by defining the radius of the circular envelope circumscribing the fingers minus the initial radius of the drop. Examples for the two drops in Fig. 11 are plotted in Fig. 12. The fingers follow a power law growth in time, with an exponent of 0.66 and 0.70 for spreading on a thin and thick film, respectively. The difference between these two exponents lies within the experimental error in digitizing the patterns. The proportionality constant is larger for the case of spreading on the thicker water film since viscous dissipation effects are smaller. In order to predict such growth laws theoretically, we intend to go beyond the linear stability analysis performed in ref. 24 to address the non-linear growth regime. We have also begun to study the fractal dimension of the fingering contours. Preliminary results indicate a perimeter fractal dimension consistent with 1.7 for spreading on different thickness films for fairly developed patterns. This result further confirms the analogy with other systems undergoing dendritic growth.

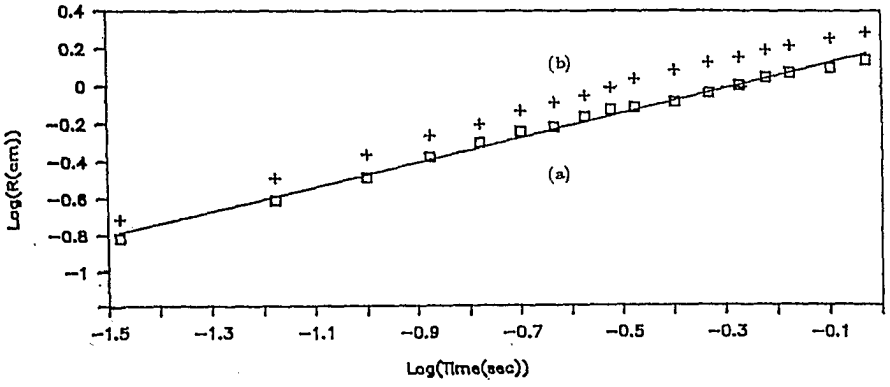

Fig. 12 Log-log plot of the fingering drop radius as a function of time. The squares and crosses correspond to the spreading of the drops in Fig. 11a and 11b, respectively. The solid line is a linear fit to the experimental data. The slopes obtained from the fits are (a) 0.66 and (b) 0.70.

In conclusion, we expect this instability to be present in many other thin film systems able to sustain large gradients in surface tension and should be of interest to those working in the exciting area of the dynamics of wetting.

ACKNOWLEDGEMENTS

This work is the co-operative effort of three authors in different laboratories. Martin Cohen Stuart would like to acknowledge P.G. de Gennes and A.M. Cazabat for receiving him kindly for a stay at the College de France, Paris and for introducing him into the subject of wetting dynamics. Sjaak Elmendorp acknowledges F. During for help with experiments and Sandra Troian wishes to thank her collaborators at Exxon : Xiao-Lun Wu, Eric Herbolzheimer and Sam Safran.

REFERENCES

1. De Gennes, P.G., Rev. Mod. Phys. **57** (1985), 827.
2. Lelah, M., Marmur, A., J. Colloid Interface Sci **82** (1981) 518.
3. Marmur, A., Adv. Colloid Interface Sci. **19** (1983), 75.
4. Cohen Stuart, M.A., Cazabat, M.A., Progr. Colloid Pol. Sci. **74**, 64 (1987); Bayramli, E., Van de Ven, T.G.M., Mason, S.G., Coll. Surf. **3**, 131 (1981).

5a. Cazabat, A.M., Cohen Stuart, M.A., J. Phys. Chem. **90** (1986), 5845.
5b. Cazabat, A.M., Cohen Stuart, M.A., C.R. Acad. Sc. Paris t **301**, II, 1337 (1985).

6. Lopez, J., Miller, C.A., Ruckenstein, E., J. Colloid Interface Sci. **56** (1976), 460.
7. Deryagin, B., Kolloidn. Zh. **17** (1955), 191.
8. Tanner, L., J. Phys. D **12** (1979), 1473.
9. Huh, C., Scriven, L.E., J. Colloid Interface Sci. **35** (1971), 85.
10. Boender, W., Chester, A.K. preprint
11. Hervet, H., De Gennes, P.G., C.R. Acad. Sci. **299II** (1984), 499.
12. Cazabat, A.M., Cohen Stuart, M.A., C.R. Acad. Sci. **301II** (1985) 1337.
13. Cazabat, A.M., Cohen Stuart, M.A., Progr. Colloid Pol. Sci. **74** (1987) 69.
14. Leger, L., Erman, M., Guinet-Picard, A.M., Ausserré, D., Strazielle, C., Benattar, J.J., Rieutord, F. Daillant, J., Bosio, L., Rev. Phys. Appl., **23** (1988) 1047.
15. Joanny, J.F., thesis, Paris, 1985.
16. Elmendorp, S., unpublished result.
17. Levinson, P., Cazabat, A.M., Cohen Stuart, M.A., Heslot, F., Nicolet, S., Rev. Phys. Appl., **23** (1988) 1009.
18. Bird, R.B. et al. "Dynamics of Polymeric Liquids", Acad. Press.
19. Burley, R. and Kennedy, B.S. in "Wetting, Spreading and Adhesion", J.F. Padday, ed. Acad. Press (1978).
20. Kennedy, B.S., Ph.D. Thesis, Herriot-Watt University, Edinburgh, Boger, D.V., J. Non Newt. Fluid Mech. **3**, 87 (1977/1978)
21. Troian, S.M., Wu, X-L, Safran, S.A., Phys. Rev. Lett, **62**, 1496 (1989).
22. Marmur, A., Lelah, M.D., Chem. Eng. Comm. **13**, 133 (1981).
23. Homsy, G.M., Ann. Rev. Fluid Mech. **19**, 271 (1987).
24. Troian, S.M., Herzbolzheimer, E., Safran, S.A., submitted to Phys. Rev. Lett.
25. Saffman, P.G., Taylor, G.I., Proc. Roy. Soc. A **245**, 312 (1958).
26. Levich, V.G. and Krylov, V.S., Ann. Rev. Fluid. Mech., **1**, 293 (1969).